ENCIT 2018

ABCM Associação Brasileira de Engenharia e Ciências Mecânicas

17th Brazilian Congress of Thermal Sciences and Engineering
November 25th-28th, 2018, Águas de Lindóia, SP, Brazil

ENCIT-2018-0576
PORE-SCALE SIMULATION OF DISPLACING IMMISCIBLE FLUIDS IN A SECOND ORDER OF SIERPINSKI CARPET POROUS MEDIA USING A LATTICE-BOLTZMANN METHOD.

Ricardo Leite Martins Bazarin
Research Center for Rheology and Non-Newtonian Fluids (CERNN), Federal University of Technology - Paraná (UTFPR), Curitiba, Brazil.
ricardoleitemartins@hotmail.com

Christian Naaktgeboren
Federal University of Technology - Paraná, Guarapuava, Brazil
NaaktgeborenC@utfpr.edu.br

Silvio Luiz de Mello Junqueira
Research Center for Rheology and Non-Newtonian Fluids (CERNN), Federal University of Technology - Paraná (UTFPR), Curitiba, Brazil.
silvio@utfpr.edu.br

Abstract. *The Lattice-Boltzmann method, which uses pseudo-potential model to describe interfacial dynamics, is used to simulate immiscible multiphase flow in porous media. The porous medium is represented by the second order of the Sierpinski carpet fractal geometry, being a geometry commonly used in the representation of porous media. The influence of capillary number (Ca) and viscosity ratio (M) is studied systematically. In the neutral displacement, we have identified three different states, stable displacement, viscous fingering, and capillary fingering, of which all are dependent of the capillary number and viscosity ratio. Analyzing the sweep efficiency by increasing capillary number in the range of* $10^{-4} \leq Ca \leq 10^{-2}$. *Sweep efficiency also increase along with the transition between different displacement states. For* $1/10 \leq M \leq 20$ *the viscosity ratio increases with the sweep efficiency, as for high values of capillarity number the transition between different displacement states occurs. The results obtained numerically in the present work agree with the experimental results of Zhang* et al. *(2011), verifying the representation of the fluid displacement process.*

Keywords: *displacement, Lattice-Boltzmann method, capillary number, viscosity ratio, sweep efficiency*

1. INTRODUCTION

Problems involving the interaction of immiscible fluids in contact with solid substrates are present both in nature as in industrial processes. In the interaction interface of the immiscible fluids in contact with solid substrate occur surface phenomena that represent macroscopic effects, such as wettability and capillarity, which are widely studied in Literature.

In the petroleum industry such phenomenon is characterized specifically in the secondary stage of the oil recovery process, where a fluid is injected into the reservoir in order to displace all petroleum present in the porous formation.

According to Chavent and Jaffré (1986), the secondary stage allows the recovery of up to 40% of the oil present at the beginning of this stage, although results of by Muggeridge *et al.* (2014) indicates a recovery of up to 70%. However, the fractions of oil recovered in the secondary stage are influenced by the fact that the injected fluid does not reach all the regions of the reservoir. Remarkably, in the regions reached part of the oil remains retained in the porous medium by the action of the wetting and capillary effects. The influence of these effects on the oil displacement behavior is complex and varies according to the characteristics of the reservoir and the fluid injection process.

The displacement of immiscible fluids through porous media involves the competition of capillary and viscous forces. The capillary forces act locally at the fluid interface and the viscous forces act throughout the fluid phase. The ratio between the viscous and capillary forces, and the viscous forces between the fluids, are represented by the capillary number

$$Ca = \frac{U_{ref}\mu}{\gamma} \tag{1}$$

and viscosity ratio

$$M = \frac{\mu_{fi}}{\mu_{fd}}, \tag{2}$$

respectively, where U_{ref} is the reference velocity, μ represents the fluid viscosity, γ is the interfacial tension between the fluids and the subindices fi e fd represent the injected fluid and the displaced fluid, respectively (Lenormand *et al.*, 1988).

According to Lenormand *et al.* (1988) three different states of displacement can be observed: viscous fingering, capillary fingering and stable displacement. In Figure (1) one observes the illustration of the states in a two-dimensional porous medium, where the arrow indicates the injection surface of the fluid. Visually viscous fingering state (a) is characterized by the formation of multiple fingers advancing towards the flow by percolating the channel with a width of pore diameter scale. The capillary fingering state (b) is represented by multiple fingers spreading through the pores in all directions, even against the direction of the displacement, forming recirculation regions. Finally, the stable displacement (c) state is characterized by a flat flow front with some irregularities occuring in the pore diameter scale.

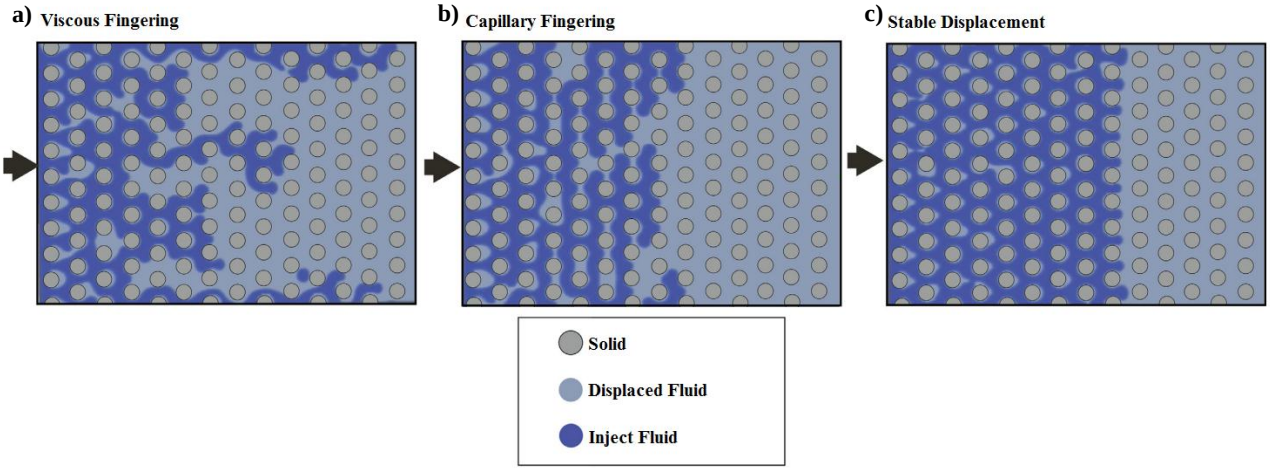

Figure 1. States of displacement in porous medium. Adapted from Tsuji *et al.* (2016).

The indication of the displacement states can be made through the diagram presented in Figure (2) credited to Lenormand *et al.* (1988), in terms of the dimensionless parameters of viscosity ratio and capillary number.

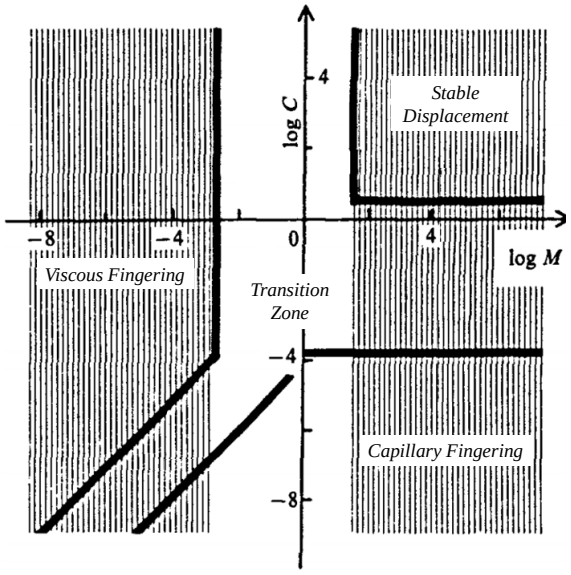

Figure 2. Diagram of displacement states. Adapted from Lenormand *et al.* (1988).

Therefore, the present work seeks the development of a numerical code capable of representing the process of fluid displacement in the different states of displacement. The numerical study is based on the Lattice Boltzmann, which is a reference method in the study of flow in porous media.

2. PROBLEM FORMULATION

In this work, the analysis of the interaction of immiscible fluids flowing in the porous medium is carried out through the study of the displacement of a fluid present in a porous channel by the injection of another fluid. The geometry corresponds to a channel of length L formed by two parallel plates filled by heterogeneous porous modeled as the second order of the Sierpinski carpet gometry. Notably, such geometry of the Sierpinbski carpet is a fractal geometry commonly used in the representation of porous media (Dullien, 1991; Jian-Hua and Bo-Ming, 2011; Bazarin *et al.*, 2017). The Figure (3) illustrates the fluid displacement process, where fluid 1 is injected with a constant parabolic velocity profile, displacing the fluid present in the porous channel.

Both fluids are assumed Newtonian for an incompressible flow (ρ_1 and ρ_2 constant). The gravitational force is negligible, being the neutral displacement represented by the intermediate wettability of the porous medium.

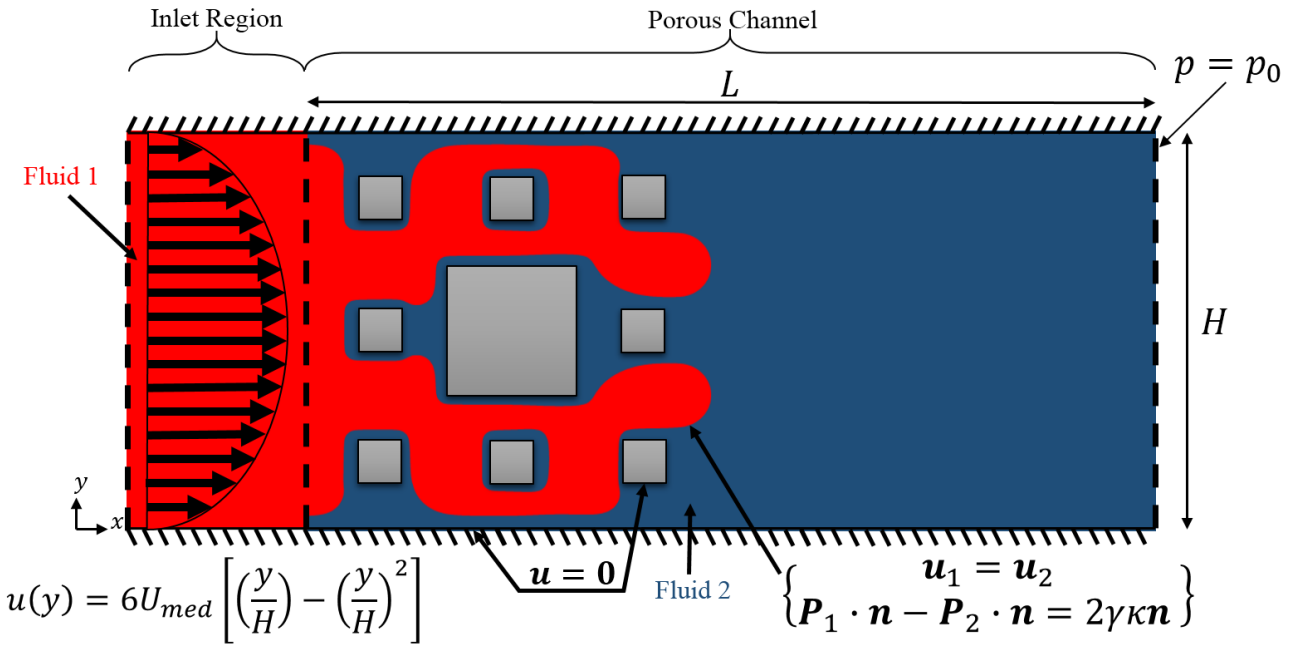

Figure 3. Geometry and boundary conditions of the problem.

The conservation equations of mass and momentum in the incompressible form of the problem are in agreement with Hilfer and Øren (1996) and are expressed, respectively, by

$$\boldsymbol{\nabla_x} \cdot (\boldsymbol{u}_\sigma) = 0, \tag{3}$$

$$\rho_\sigma \frac{\partial \boldsymbol{u}_\sigma}{\partial t} + \rho_\sigma (\boldsymbol{u}_\sigma \cdot \boldsymbol{\nabla_x}) \boldsymbol{u}_\sigma = -\boldsymbol{\nabla_x} p_\sigma + \rho_\sigma \nu_\sigma \boldsymbol{\nabla_x^2} \boldsymbol{u}_\sigma + \rho_\sigma \boldsymbol{g}, \tag{4}$$

where σ indicates the respective fluid, $\boldsymbol{u}$ the velocity vector, t the time, p the pressure, $\boldsymbol{g}$ the external force per unit of mass and the term $\boldsymbol{\nabla_x^2}$ represents the scalar product $\boldsymbol{\nabla_x} \cdot \boldsymbol{\nabla_x}$.

Initially the problem is characterized by an inlet region filled by fluid 1, while the porous channel remains saturated by fluid 2, both fluids with zero velocity field. The boundary conditions are parabolic velocity profile at the entrance and constant pressure at the channel exit, non-slip conditions are also applied to the walls and surfaces of the blocks. The boundary conditions are also required at the interaction interface of the immiscible fluids in order to guarantee momentum conservation:

$$\boldsymbol{u}_1 = \boldsymbol{u}_2 \quad \text{e} \quad \boldsymbol{P}_1 \cdot \boldsymbol{n} - \boldsymbol{P}_2 \cdot \boldsymbol{n} = 2\gamma\kappa\boldsymbol{n}, \tag{5}$$

where $\boldsymbol{n}$ is the unit normal vector, κ is the curvature of the interface and $\boldsymbol{P}$ is the pressure tensor, given by

$$\boldsymbol{P} = p\boldsymbol{I} + \mu \frac{1}{2} \left(\boldsymbol{\nabla_x} \boldsymbol{u} + \boldsymbol{\nabla_x} \boldsymbol{u}^T - \frac{2}{3} (\boldsymbol{\nabla_x} \cdot \boldsymbol{u}) \boldsymbol{I} \right). \tag{6}$$

Such a representation of the boundary conditions at the interface of the fluids, described by Hilfer and Øren (1996), is characterized by a singular interface where the phase interface is modeled by means of a discontinuity surface, i.e., the phase transition region has no thickness (Leal, 2007). An illustration of the boundary conditions can be seen in Figure (3).

The sweep efficiency is the main analysis parameter of the present work, representing the efficiency of the displacement process of immiscible fluids, given by

$$Se = \frac{V_{fi}}{V_p} \tag{7}$$

where Se is the sweep efficiency, V_{fi} is the volume occupied by the injected fluid and V_p is the pore volume.

3. NUMERICAL PROCEDURE

The numerical formulation of the problem is done by the Lattice-Boltzmann method, which consists of a discrete form of the Boltzmann equation in space velocity and space-time. The method is represented by the evolution of the distribution function f which describes the probability of a particle to be in a certain position at a certain speed at a specific time (Abe, 1997; He and Luo, 1997). For the representation of the multiphase system the present work uses the pseudo-potential model, developed by Shan and Chen (1993), with some changes proposed by Porter *et al.* (2012). The pseudo-potential model is based on the potential interaction of the particles of each phase, represented by forces resulting from the density variation.

The Boltzmann discretized equation, given by the Equation (8), called the Lattice-Boltzmann equation, is represented in the present work using the model proposed by Bhatnagar *et al.* (1954) for simplification of the integral-differential collision operator:

$$f_{i,\sigma}(\boldsymbol{x} + \boldsymbol{e}_i\delta_t, t + \delta_t) = f_{i,\sigma}(\boldsymbol{x}, t) - \frac{1}{\tau_\sigma}(f_{i,\sigma}(\boldsymbol{x}, t) - f^{eq}_{i,\sigma}(\boldsymbol{x}, t)) + \left(1 - \frac{1}{2\tau_\sigma}\right)\delta_t F_{i,\sigma}(\boldsymbol{x}, t), \tag{8}$$

where f^{eq} is the equilibrium distribution function, F_i is the force term, $\boldsymbol{e}$ is the velocity particle vector, i represents the index of space velocity discretization, δ_t is the discrete time increment and τ represents the non-dimensional relaxation time given by

$$\tau_\sigma = \frac{\nu_\sigma}{c_s^2} + \frac{1}{2}, \tag{9}$$

where c_s represents the sound speed in the method scale.

The equilibrium distribution function, present in Equation (8) is given by the Maxwell-Boltzmann distribution function, which represents the probability of a particle at a steady state. Using a second order discretization of velocity space, the equilibrium distribution function is represented by the Equation (10) in its discretized form and truncated in the second order term (Philippi *et al.*, 2006):

$$f^{eq}_{i,\sigma} = \rho_\sigma w_i\Big(1 + \frac{\boldsymbol{e}_i \cdot \boldsymbol{u}_\sigma}{c_s^2} + \frac{1}{2c_s^4}\boldsymbol{u}_\sigma\boldsymbol{u}_\sigma\colon(\boldsymbol{e}_i\boldsymbol{e}_i - c_s^2\boldsymbol{I})\Big), \tag{10}$$

where w_i are the weight factors for the corresponding index of space velocity discretization.

The force term, represented by the scheme proposed by He *et al.* (1998), consists of the approximation of the distribution function by the equilibrium distribution function, given by

$$F_{i,\sigma} = \frac{\boldsymbol{\mathcal{F}}_\sigma}{\rho_\sigma} \cdot \boldsymbol{\nabla}_{\boldsymbol{\xi}} f_{i,\sigma} \approx \frac{\boldsymbol{\mathcal{F}}_\sigma}{\rho_\sigma} \cdot \boldsymbol{\nabla}_{\boldsymbol{\xi}} f^{eq}_{i,\sigma} = \frac{\boldsymbol{\mathcal{F}}_\sigma}{\rho_\sigma} \cdot \frac{\boldsymbol{e}_i - \boldsymbol{u}_\sigma}{c_s^2} f^{eq}_{i,\sigma}, \tag{11}$$

where $\boldsymbol{\mathcal{F}}$ is the external force per unit of volume. The evolution of the dynamic interface of the different phases in the pseudo-potential model occurs by the fluid cohesion force that is based on the methodology of Shan (2006) for a tenth-order approximation, represented by equation

$$\boldsymbol{\mathcal{F}}_{c,\sigma} = -G_c\rho_\sigma(\boldsymbol{x}, t)c_s^2\sum_i w(|e_i|^2)\rho_{\overline{\sigma}}(\boldsymbol{x} + \boldsymbol{e}_i\delta, t)\boldsymbol{e}_i \tag{12}$$

where $\boldsymbol{\mathcal{F}}_{c,\sigma}$ represents the cohesion force, $w(|e_i|^2)$ the weights for each order of approximation and $\overline{\sigma}$ the opposite phase of σ. The cohesion coefficient G_c is an important parameter, as it controls the intensity of the cohesion force and consequently the immiscibility of the fluids.

The macroscopic properties of the problem are recovered from the momentum of the distribution functions, i.e.,

$$\rho_\sigma = \sum_i f_{i,\sigma} \quad \text{and} \quad \rho_\sigma\boldsymbol{u}_\sigma = \sum_i \boldsymbol{e}_i f_{i,\sigma} + \frac{\delta_t}{2}\boldsymbol{\mathcal{F}}_\sigma. \tag{13}$$

The discretization of the velocity space is done using a second-order approximation for nine points, obtaining the two-dimensional lattice D2Q9 (see Figure (4)), where

$$\begin{aligned} \boldsymbol{e}_{i=0} &= (0,0), \\ \boldsymbol{e}_{i=1,2,3,4} &= \left(\cos\frac{i-1}{2}\pi, \sin\frac{i-1}{2}\pi\right), \\ \boldsymbol{e}_{i=5,6,7,8} &= \sqrt{2}\left(\cos\frac{i-5}{2}\pi + \frac{\pi}{4}, \sin\frac{i-5}{2}\pi + \frac{\pi}{4}\right). \end{aligned} \tag{14}$$

The D2Q9 lattice weight factors are given by $\omega_0 = 4/9$, $\omega_i = 1/9$ for $i = 1, 2, 3, 4$; and $\omega_i = 1/36$ for $i = 5, 6, 7, 8$; and the sound speed by $c_s = 1/\sqrt{3}$.

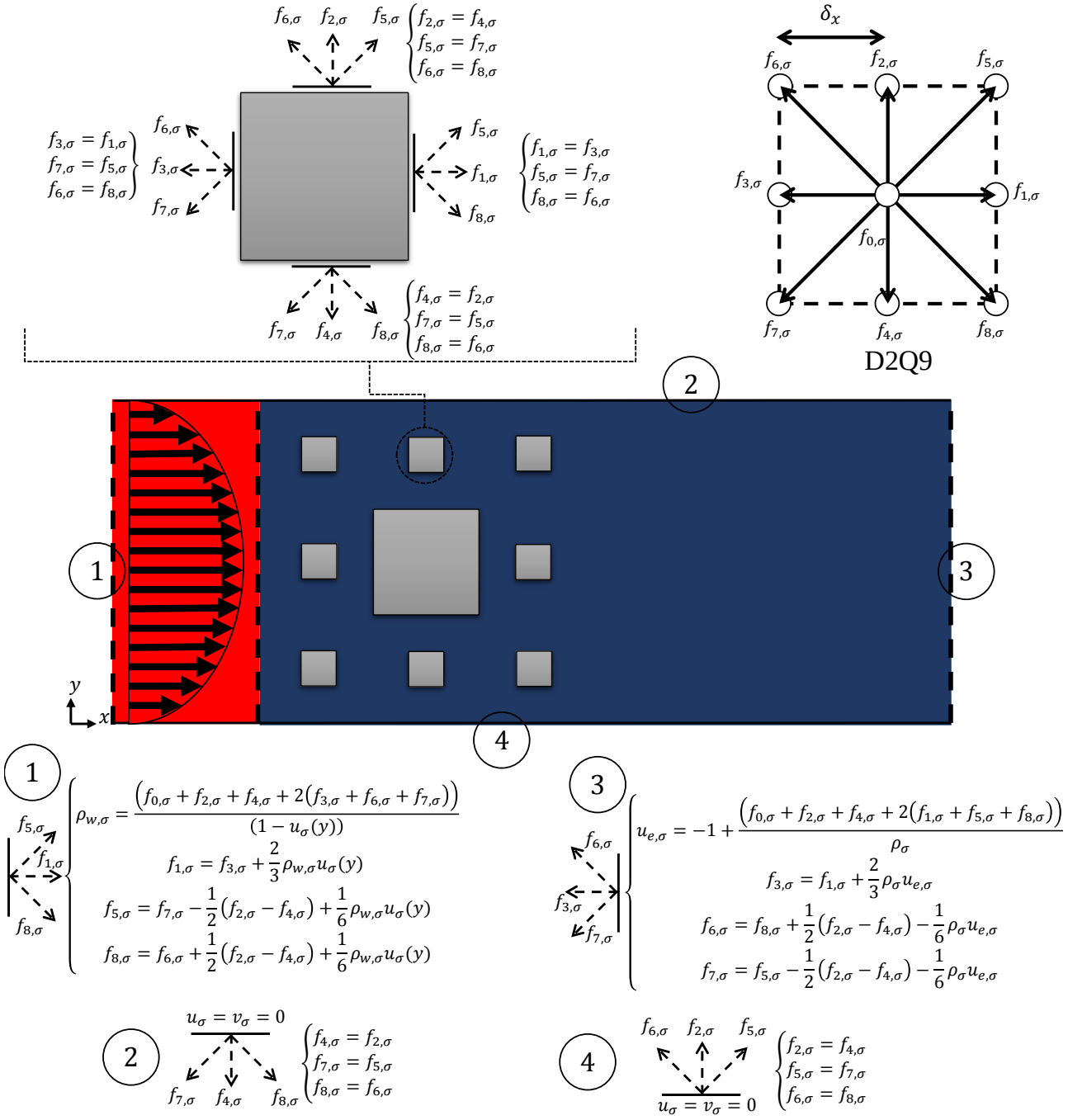

Figure 4. Boundary conditions of the problem in the Lattice-Boltzmann Method.

3.1 Boundary Conditions

The non-slip conditions on solid surfaces is done via the lattice bounce-back model for a second order accuracy (Krüger *et al.*, 2017). Additionally, the boundary conditions of constant velocity and pressure are considered at the channel inlet and outlet regions, respectively. Such conditions are represented using the model proposed by Zou and He (1997), which is based on the tension tensor symmetry and expressed algebraically by

$$f_i^{neq} = f_i - f_i^{eq} = f_{i'} - f_{i'}^{eq} = f_{i'}^{neq} \tag{15}$$

where f^{neq} is the non-equilibrium distribution function and i' is the opposite direction to i. The application of the boundary conditions at the boundaries and surfaces of the blocks are highlighted in Figure (4).

The boundary conditions at the interface between fluids 1 and 2, as described by Hilfer and Øren (1996), are represented by the pseudo-potential model based on the diffuse interface theory, where the dynamic fluid interface is approached thermodynamically (Sbragaglia *et al.*, 2007).

3.2 Grid Test

The test seeks to minimize the total error related to the method given by the sum of $E_{total} = E_{\mathrm{Ma}} + E_{\delta_x} + E_{\delta_t}$, where E_{total} is the total error, E_{Ma} is the error associated with compressibility (Ma is the Mach number), E_{δ_t} is the temporal error associated with the time step and E_{δ_x} is the spatial error associated with the mesh ($\delta_x = \boldsymbol{e}_i \delta_t$ is the lattice spacing). The determination of δ_x and δ_t is given by the ratio between the real scale of the problem and the method scale, following the methodology proposed by Latt (2008).

The error related to compressibility to $\mathrm{Ma} < 1$ is order of magnitude Ma^2, calculated by $\mathrm{Ma} = |\boldsymbol{u}|/c_s$ in the lattice-Boltzmann scale. From the established compressibility error, the relationship between the errors is given by

$$E_{\mathrm{Ma}} \propto \frac{E_{\delta_t}}{E_{\delta_x}} \propto \frac{1}{r^2} \tag{16}$$

where E_{δ_x} is of the order δ_x^2, E_{dt} of order δ_t^2 and $r = \delta_x/\delta_t$ is a ratio between the lattice spacing and the time increment. For more details on the test methodology see Meira (2016) and Meira *et al.* (2017).

4. RESULTS AND DISCUSSION

For this study, two fluids of the same density $\rho_1 = \rho_2 = 800[kg/m^3]$ and viscosities $\nu_2 = 10^{-3}[m^2/s]$ and $\nu_1 = 10^{-3}/M[m^2/s]$, are defined. It is emphasized that the fluid 2 have the properties of light oil, while the kinematic viscosity of the fluid 1 is varied as a function of the viscosity ratio.

For the analyzed cases the capillary number is calculated as a function of the displaced fluid viscosity and the maximum velocity of the parabolic inlet profile, i.e,

$$Ca = \frac{\mu_2 U_{max}}{\gamma}. \tag{17}$$

To characterize the immiscible fluid displacement process, the cohesion coefficient is chosen within the range of immiscibility for $G_c = 4$, corresponding to interfacial tension $\gamma = 0,14[Pa.m]^{LB}$, where the superscript LB indicates the method scale, for more details see Latt (2008). Given a value of the fluid interfacial tension, the scales are dealed so that the viscosity of the injected fluid is $\mu_2 = 0,14[m^2/s]^{LB}$, simplifying the application of the capillary number to

$$Ca = U_{max}. \tag{18}$$

The variation, in the analyzed displacemente process of the capillary number and viscosity ratio parameters, are established in Table 1 based on a numerical code pre-analysis. For values of $Ca \geq 10^{-1}$ a high Mach number is observed for the flows through the porous medium, where compressibility effects introduce numerical errors. However, for $Ca < 10^{-4}$ the reduced flow velocities result in a large number of iterations to observe the displacement and, consequently, a high computational cost that makes the simulations impracticable. In the values of the viscosity ratio it was observed that the simulated range for the displacement process is $1/10 \leq M \leq 20$, so that values above or below this range turn the simulation unstable.

When applied the grid test mentioned earlier, on variations in sweep efficiency over the time. Applied in the critical case of $Ca = 10^{-2}$ and $M = 20$, the reference mesh obtained corresponds to $H = 144[m]^{LB}$ and $L = 576[m]^{LB}$.

In Figure (5), the results can be observed at the point of constant scanning efficiency. The injected fluid, the displaced and the solid one are represented graphically by the colors white, black and gray, respectively.

According to the range of the parameters of capillary number and viscosity ratio, established in Table 1, and the ranges observed in a literature review, one can verify a proximity to the range studied experimentally by Zhang *et al.* (2011). Figure (6) illustrates both analysis ranges. Despite the similarity of the bands shown in Figure (6), it is emphasized that different porous media and different fluids were used in both works.

Table 1. Range of parameters investigated.

Parameters		Values.
Viscosity Ratio	M	$1/10$, 1, 10, 20
Capillary Number	Ca	10^{-2}, 5.10^{-2}, 10^{-3}, 5.10^{-3}, 10^{-4}

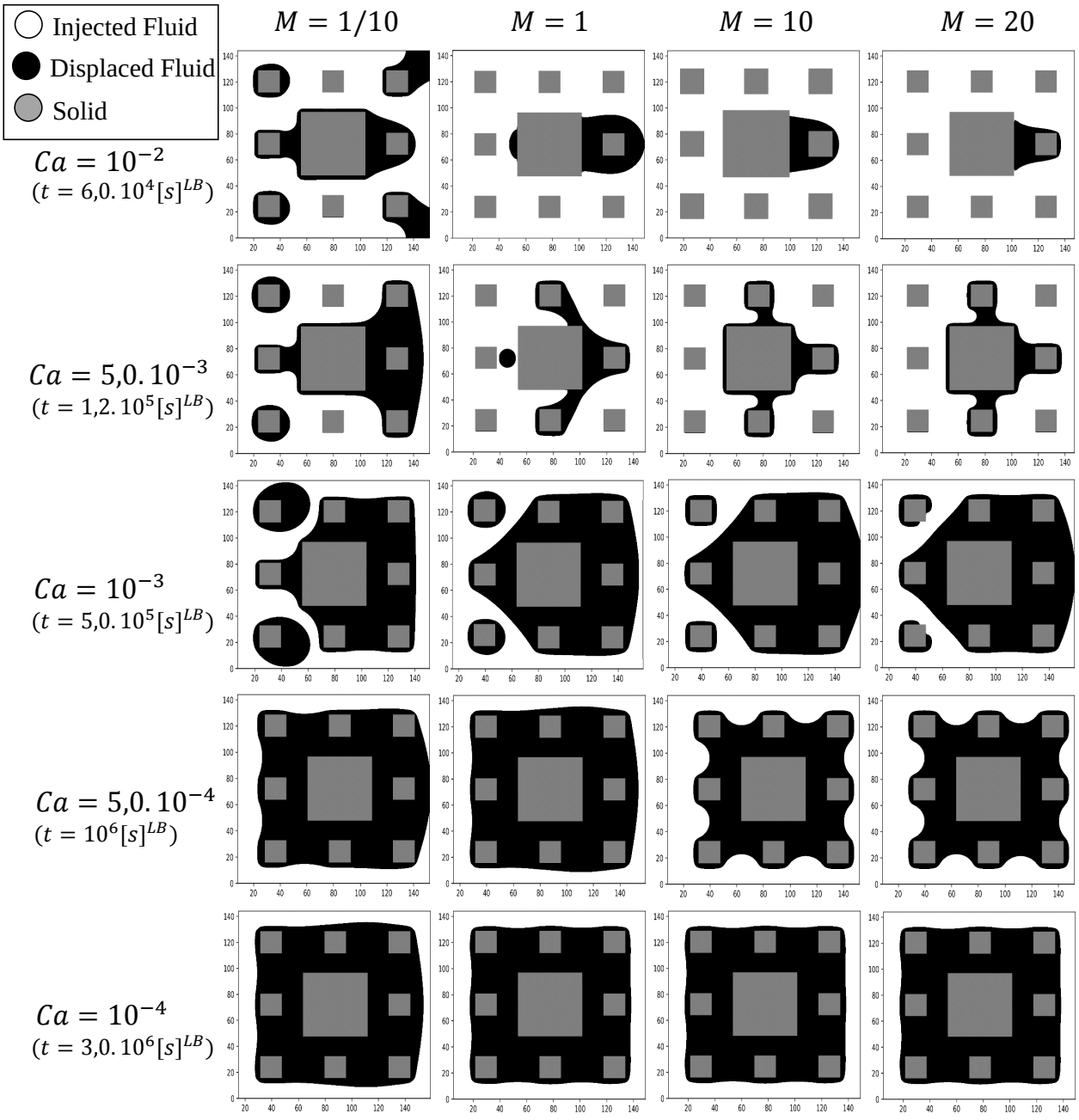

Figure 5. Representation of the displacement process for the range of the capillary number and viscosity ratio at the point of constant sweep efficiency ($t = [s]^{LB}$).

4.1 Analysis of the Capillary Number

Observe in Figure (5) that the sweep efficiency capillary tends to be reduced with the capillary number, as well as a change on the topology of the fluid retained (highlighted in black color) resulting from the transition of the fluid displacement state. In Figure (7) the values of the sweep efficiency in function of the capillary number, are observed for each viscosity ratio. Comparing the values obtained with the results of Zhang *et al.* (2011) a similar behavior occurs, since both results indicate that the sweep efficiency reduces with the capillary number, for all values of viscosity ratio. Note also, in the present results a large decrease in the scanning efficiency of $Ca = 5,0.10^{-3}$ to $Ca = 10^{-3}$, due to the

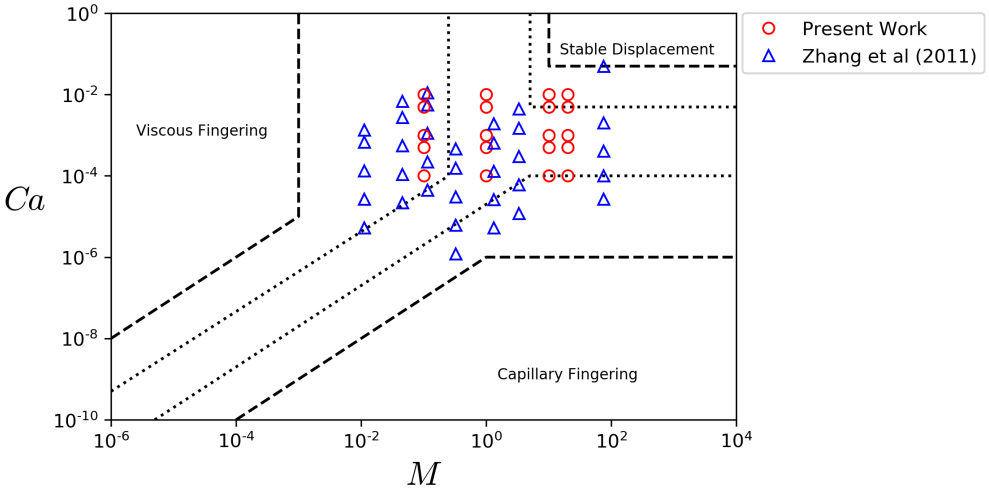

Figure 6. Range of parameters investigated in the diagram by Zhang *et al.* (2011) and by the present work.

transition point of the domain between capillary and viscous forces in the fluid displacement process.

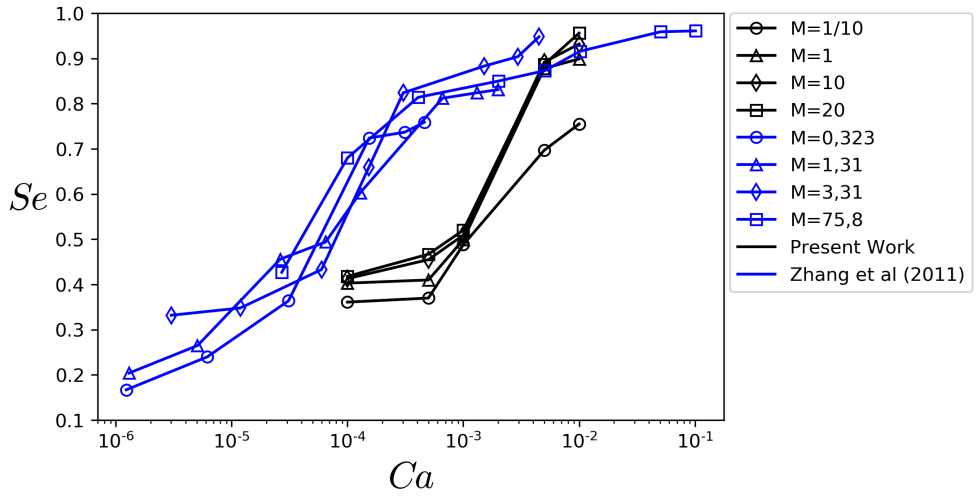

Figure 7. Sweep efficiency values as a function of the capillary number, obtained by the present work and compared with Zhang *et al.* (2011), for different viscosity ratios.

4.2 Analysis of the Viscosity Ratio

Results for the viscosity ratio with constant capillary number are analyzed in Figure (8). One can observe the growth of the sweep efficiency with the viscosity ratio for all values of the capillary number. However, unlike the capillary number analysis where all ranges show transitions between the displacement states, the viscosity ratio variation exhibits transition only to $Ca = 10^{-2}$, so that, for $Ca \leq 5, 0.10^{-3}$ the displacements show similar states.

Figure (8) displays the values of the sweep efficiency as a function of the viscosity ratio for each number of capillarity. One can verify the growth of the sweep efficiency with the viscosity ratio. The results obtained by Zhang *et al.* (2011), have a tendency of increase of the sweep efficiency with the viscosity ratio is observed, as well as in the present work.

5. Conclusion

Based on the problem numerically developed for representing the fluid displacement process through porous media, the results obtained show an expected behavior in the range analyzed with the results obtained experimentally by Zhang *et al.* (2011). However, some limitations concerning to the Lattice-Boltzmann method with the pseudo-potential model were observed to the capillary number and viscosity ratio parameters, so that the ranges of $Ca \geq 10^{-1}$, $M \geq 20$ and $M \leq 1/10$, are not simulated due to method instability. Nevertheless, it is possible that such simulation ranges can be extended using techniques of regularization of the method and larger orders of discretization of both space-time and

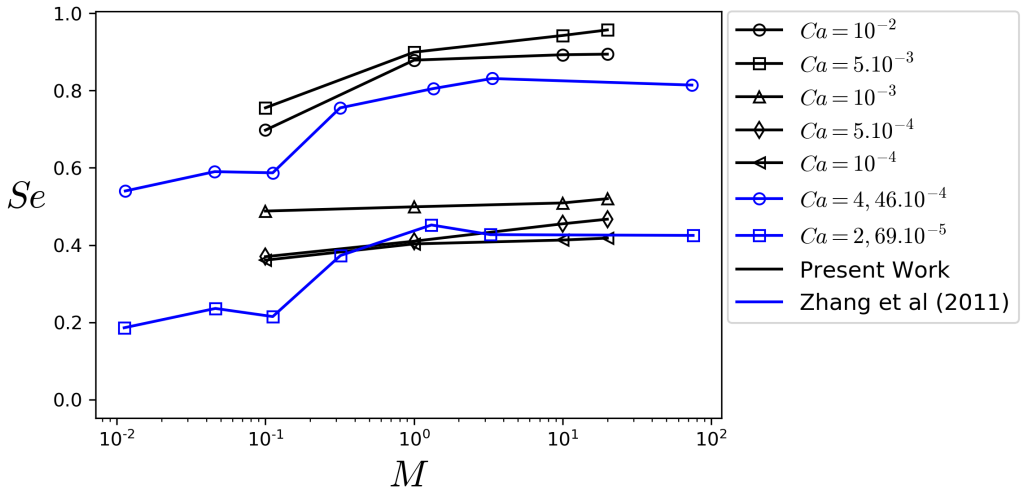

Figure 8. Sweep efficiency values as a function of the viscosity ratio, obtained by the present work and compared with Zhang *et al.* (2011), for different capillarity numbers.

velocity space.

In the analysis of the range of Ca and M, the growth of Se is observed for both the increase of Ca and the increase of M. It was also observed the transition between different displacement states, which represent the states of fingering viscous, capillary fingering and stable displacement.

6. ACKNOWLEDGEMENTS

The authors would like to acknowledge the support of REPSOL, the PRH-ANP/MCT program (PRH10-UTFPR) and the National Council for Scientific and Technological Development (CNPq).

7. REFERENCES

Abe, T., 1997. "Derivation of the lattice boltzmann method by means of the discrete ordinate method for the boltzmann equation". *Journal of Computational Physics*, Vol. 131, No. 1, pp. 241 – 246. ISSN 0021-9991. doi:http://dx.doi.org/10.1006/jcph.1996.5595. URL `http://www.sciencedirect.com/science/article/pii/S0021999196955953`.

Bazarin, R.L.M., Naaktgeboren, C. and Junqueira, S.L.M., 2017. "Lattice-boltzmann assessment of the tortuosity af a 2d sierpinski carpet type of porous medium". In *Proceedings of the 24st International Congress of Mechanical Engineering - COBEM2017*. Curitiba, Brazil.

Bhatnagar, P.L., Gross, E.P. and Krook, M., 1954. "A model for collision processes in gases. i. small amplitude processes in charged and neutral one-component systems". *Phys. Rev.*, Vol. 94, pp. 511–525. doi:10.1103/PhysRev.94.511. URL `http://link.aps.org/doi/10.1103/PhysRev.94.511`.

Chavent, G. and Jaffré, J., 1986. *Mathematical models and finite elements for reservoir simulation: single phase, multiphase and multicomponent flows through porous media*, Vol. 17. Elsevier.

Dullien, F.A., 1991. "Porous media: fluid transport and pore structure".

He, X. and Luo, L.S., 1997. "Theory of the lattice boltzmann method: From the boltzmann equation to the lattice boltzmann equation". *Phys. Rev. E*, Vol. 56, pp. 6811–6817. doi:10.1103/PhysRevE.56.6811. URL `http://link.aps.org/doi/10.1103/PhysRevE.56.6811`.

He, X., Shan, X. and Doolen, G.D., 1998. "Discrete boltzmann equation model for nonideal gases". *Physical Review E*, Vol. 57, No. 1, p. R13.

Hilfer, R. and Øren, P., 1996. "Dimensional analysis of pore scale and field scale immiscible displacement". *Transport in Porous Media*, Vol. 22, No. 1, pp. 53–72.

Jian-Hua, L. and Bo-Ming, Y., 2011. "Tortuosity of flow paths through a sierpinski carpet". *Chinese Physics Letters*, Vol. 28, No. 3, p. 034701.

Krüger, T., Kusumaatmaja, H., Kuzmin, A., Shardt, O., Silva, G. and Viggen, E.M., 2017. *The Lattice Boltzmann Method*. Springer.

Latt, J., 2008. "Choice of Units in Lattice Boltzmann Simulation". Wiki.palabos.org/_media/howtos:lbunits.pdf.

Leal, L.G., 2007. *Advanced transport phenomena: fluid mechanics and convective transport processes*, Vol. 7. Cambridge University Press.

Lenormand, R., Touboul, E. and Zarcone, C., 1988. "Numerical models and experiments on immiscible displacements in porous media". *Journal of fluid mechanics*, Vol. 189, pp. 165–187.

Meira, R.E.C.P., 2016. "Pore-scale simulations of gas displacing liquid in a homogeneous pore network using the lattice boltzmann method".

Meira, R.E.C.P., De Lai, F.C., Negrao, O.R. and Junqueira, S.L.M., 2017. "Numerical analysis of power law fluid flow in a channel partially filled by a porous medium using the lattice boltzmann method". In *Proceedings of the 24st International Congress of Mechanical Engineering - COBEM2017*. Curitiba, Brazil.

Muggeridge, A., Cockin, A., Webb, K., Frampton, H., Collins, I., Moulds, T. and Salino, P., 2014. "Recovery rates, enhanced oil recovery and technological limits". *Phil. Trans. R. Soc. A*, Vol. 372, No. 2006, p. 20120320.

Philippi, P.C., Hegele Jr, L.A., Dos Santos, L.O. and Surmas, R., 2006. "From the continuous to the lattice boltzmann equation: the discretization problem and thermal models". *Physical Review E*, Vol. 73, No. 5, p. 056702.

Porter, M.L., Coon, E., Kang, Q., Moulton, J. and Carey, J., 2012. "Multicomponent interparticle-potential lattice boltzmann model for fluids with large viscosity ratios". *Physical Review E*, Vol. 86, No. 3, p. 036701.

Sbragaglia, M., Benzi, R., Biferale, L., Succi, S., Sugiyama, K. and Toschi, F., 2007. "Generalized lattice boltzmann method with multirange pseudopotential". *Physical Review E*, Vol. 75, No. 2, p. 026702.

Shan, X., 2006. "Analysis and reduction of the spurious current in a class of multiphase lattice boltzmann models". *Physical Review E*, Vol. 73, No. 4, p. 047701.

Shan, X. and Chen, H., 1993. "Lattice boltzmann model for simulating flows with multiple phases and components". *Physical Review E*, Vol. 47, No. 3, p. 1815.

Tsuji, T., Jiang, F. and Christensen, K.T., 2016. "Characterization of immiscible fluid displacement processes with various capillary numbers and viscosity ratios in 3d natural sandstone". *Advances in water resources*, Vol. 95, pp. 3–15.

Zhang, C., Oostrom, M., Wietsma, T.W., Grate, J.W. and Warner, M.G., 2011. "Influence of viscous and capillary forces on immiscible fluid displacement: Pore-scale experimental study in a water-wet micromodel demonstrating viscous and capillary fingering". *Energy & Fuels*, Vol. 25, No. 8, pp. 3493–3505.

Zou, Q. and He, X., 1997. "On pressure and velocity boundary conditions for the lattice boltzmann bgk model". *Physics of fluids*, Vol. 9, No. 6, pp. 1591–1598.

8. RESPONSIBILITY NOTICE

The authors are the only responsible for the printed material included in this paper.